

# An Improved Method for Spinal Functional MRI With Large Volume Coverage of the Spinal Cord

Patrick W. Stroman, PhD,<sup>1,2,3\*</sup> Jennifer Kornelsen, BA,<sup>2</sup> and Jane Lawrence, BSc<sup>2</sup>

**Purpose:** To develop a spinal functional MRI (fMRI) method with three-dimensional coverage of a large extent of the spinal cord with minimal partial volume effects

**Materials and Methods:** fMRI data of the cervical spinal cord were obtained at 1.5 T with a single-shot fast spin-echo imaging method, from thin contiguous sagittal slices spanning the cord. Thermal stimulation was applied to the palm of the hand in a block pattern with 15°C for stimulation and 32°C during baseline periods. Prior to analysis, the image data at each time point were reformatted into three-dimensional volumes and resliced perfectly transverse to the spinal cord. Smoothing was applied only in the superior-inferior (S/I) direction across uniform tissue types. Active voxels were then identified by means of a correlation to a model paradigm.

**Results:** The resulting activity maps demonstrate activity primarily in ipsilateral sensory areas and in some motor areas, consistent with the spinal cord neuroanatomy. These data also demonstrate detail of the subsegmental organization of the spinal cord, as well as anatomical detail of the spinous processes and positions of nerve roots.

**Conclusion:** The spinal fMRI method described enables large volume coverage of the spinal cord in three dimensions, with reliable and reproducible results.

**Key Words:** spinal cord; human; magnetic resonance imaging; fMRI; methods

**J. Magn. Reson. Imaging 2005;21:520–526.**

© 2005 Wiley-Liss, Inc.

FUNCTIONAL MRI (fMRI) of the human spinal cord has been demonstrated to be effective at demonstrating areas of neuronal activity in the spinal cord, in response

to an external stimulus, in both healthy and injured people (1–7). However, there are several challenges that must be overcome before this method will be sufficiently practical and reliable for use as a tool for clinical assessment or for spinal cord research. These challenges are caused by the flow of cerebrospinal fluid (CSF) around the cord, the magnetic susceptibility differences between the cord and the surrounding bone, and the relatively small cross-sectional dimensions of the cord ( $\sim 16 \times 10$  mm at the cervical enlargement) with a large superior-inferior (S/I) extent ( $\sim 45$  cm). Artifacts arising from CSF flow can be reduced with flow-compensating gradients, and the motion this imparts to the cord has been shown to be a likely source of error in spinal fMRI results (8), but this has yet to be fully addressed. The effects of susceptibility gradients have been overcome by acquiring spinal fMRI data with proton-density weighted spin-echo imaging methods. Neuronal-activity related contrast changes arise from the blood-oxygenation level dependent (BOLD) contrast, as well as from signal enhancement by extravascular water protons (SEEP) (4,9). The underlying physiological mechanism that has been proposed for SEEP is a local change in extravascular water content driven by changes in perfusion pressure and production of extracellular fluid (ECF) (4,10,11). Local water content changes related to cell swelling, and changes in the extracellular volume, may also contribute because it has been shown that these processes may play an important role in neuronal signaling (12–16). The small cross-sectional dimensions of the cord result in problems of partial volume effects or a tradeoff with the extent of the cord that can be imaged. The method that has been demonstrated to be effective for spinal fMRI employs transverse slices because this orientation is superior for distinguishing gray and white matter (less partial-volume effect) and slices can be positioned to be aligned with the centers of the vertebral bodies or the intervertebral discs, where the through-slice field homogeneity is optimal (2). However, this slice orientation provides only a limited view of the cord, with low resolution in the rostral-caudal direction. The alternative of employing sagittal or coronal slices has been employed (17–20), but the slices acquired have been one-half to one-fourth of the cord width or depth in order to achieve an adequate signal-to-noise ratio and the results have suffered from severe partial volume effects. In the

<sup>1</sup>Department of Diagnostic Radiology, Queen's University, Kingston, Ontario, Canada.

<sup>2</sup>Department of Physiology, University of Manitoba, Winnipeg, Manitoba, Canada.

<sup>3</sup>Institute for Biodiagnostics, National Research Council of Canada, Winnipeg, Manitoba, Canada.

Contract grant sponsor: Canadian Institutes of Health Research (CIHR); Contract grant sponsor: Canada Research Chairs Program.

\*Address reprint requests to: P.W.S., Dept of Diagnostic Radiology, c/o Center for Neuroscience Studies, 231 Botterell Hall, Queen's University, Kingston, Ontario, Canada K7L 2V7.  
E-mail: stromanp@post.queensu.ca

Received July 19, 2004; Accepted January 31, 2005.

DOI 10.1002/jmri.20315

Published online in Wiley InterScience (www.interscience.wiley.com).

present study, we propose that spinal fMRI data can be acquired with thin contiguous sagittal slices, with smoothing applied only across consistent tissues to increase the signal-to-noise ratio without incurring partial-volume effects.

Therefore, in this work we describe a new method, based on sagittal slices, but with several very significant differences from the methods previously used by others (18–20). This new method makes use of a single-shot fast spin-echo technique to image contiguous sagittal slices of the spinal cord that are as thin as the hardware will allow, regardless of the signal-to-noise ratio of the resulting images. The slices are then reformatted into a three-dimensional volume, and resliced perfectly transverse to the spinal cord. Smoothing is applied only in the rostral–caudal direction across consistent tissue types, and spinal fMRI analysis is applied to the resultant axial slices as per our usual method (5,6). The functional maps resulting from this method are in the form of isotropic voxels spanning a three-dimensional volume, and can be reformatted into any desired slice orientation. This permits visualization of areas of activity in relation to anatomical markers such as vertebrae, spinous processes, and spinal nerve roots. Here, we demonstrate the effectiveness and reliability of this new method, and propose that it provides the practical spinal fMRI tool needed for clinical assessment or research.

Previous spinal fMRI studies employing thermal sensory stimulation of various areas of the hand, forearm, or leg have demonstrated a consistent pattern of activity in the corresponding spinal cord segments (2,3,5,21). Activity is primarily in ipsilateral dorsal areas and projects to ipsilateral ventral regions, with some activity also in contralateral ventral areas and around the central canal (5,6). The magnitude of the signal intensity changes has also been observed to vary with the stimulation temperature, including a clear transition in the response between cold sensation, and noxious or painful cold, demonstrating the correspondence between the observed signal changes and neuronal activity (5). Recent studies in an animal model (rat) have demonstrated a close correspondence between areas of activity identified with spinal fMRI and with direct histological detection of neuronal activity (21). Signal intensity changes in the cervical spinal cord have been consistently observed to be  $6.4\% \pm 1.3\%$  (mean  $\pm$  SD) with thermal stimulation of the palm of the hand at  $15^{\circ}\text{C}$ , and  $7.0\% \pm 0.9\%$  with  $10^{\circ}\text{C}$  stimulation, in healthy volunteers (3,4). In the lumbar spinal cord, the signal intensity changes with  $10^{\circ}\text{C}$  stimulation of the leg were  $6.6\% \pm 0.9\%$  and  $7.2\% \pm 1.5\%$ , in healthy and injured subjects, respectively (5). In order to validate the new method, we have employed the same stimulus in the present study in order to elicit the same consistent pattern of response.

## MATERIALS AND METHODS

Spinal fMRI studies of seven healthy volunteers were carried out at 1.5 T in a GE Signa Horizon LX clinical MR system. In most of the subjects, experiments were duplicated and a total of 22 sets of spinal fMRI data

were obtained. Data were acquired with single-shot fast spin-echo imaging with a  $12\text{-cm} \times 12\text{-cm}$  field of view,  $128 \times 128$  matrix, and an effective echo time of 36 msec. A commercial GE phased-array spine coil was used for signal reception and a body coil was used for transmission of spatially uniform radiofrequency (RF) excitation pulses. K-space data were zero-filled to  $256 \times 256$  prior to reconstruction. Eight contiguous sagittal slices, each 2.8 mm thick, were selected to span the cord, requiring a repetition time of approximately 10 seconds. This provided a resolution of  $2.8 \times 0.9 \times 0.9$  mm (right–left [R/L]  $\times$  anterior–posterior [A/P]  $\times$  S/I), in the original image data. Thermal stimulation of the palm of the right hand was applied with a  $3\text{-cm} \times 3\text{-cm}$  thermode with temperature controlled by a Medoc TSA-II thermal sensory analyzer with input from a personal computer (PC). This was used to elicit reproducible activity in the sixth to eighth cervical spinal cord segments without incurring task-related motion. The thermode temperature was set to  $15^{\circ}\text{C}$  for stimulation and  $32^{\circ}\text{C}$  during baseline periods, with the transition occurring in one TR period (10 seconds). A block design was used with two stimulation periods of 50–60 seconds duration, interleaved with rest periods of 60–70 seconds. The total acquisition time for each experiment was 350 seconds, with the spinal cord imaged 35 times to describe the fMRI time course.

Data were analyzed using custom-made software written in MatLab (The MathWorks, Natick, MA, USA). Prior to analysis, a line was drawn manually along the anterior edge of the spinal cord in a midline sagittal image taken from the functional data set, and this was used as a reference for the spinal cord position and curvature. The sagittal slice data at each time point of the functional series were combined into a three-dimensional volume and linearly interpolated to obtain cubic voxels  $0.5 \times 0.5 \times 0.5$  mm. The volume was then resliced perfectly transverse to the spinal cord and smoothing was applied only in the rostral–caudal direction to be across consistent anatomy. The correlation between a model paradigm and the signal intensity time course of each voxel was computed in order to construct a map of correlation T-values. A T-value threshold of 2.0 was chosen to identify voxels as being active, corresponding to a P-value threshold of 0.05, and were plotted in color over a grayscale average image of the volume. An intensity threshold was set manually on the background image to identify the higher intensity CSF, and a mask was created to exclude false activations arising from within the CSF. The volume map demonstrating the areas of activity was then also reformatted back into thin sagittal slices for viewing.

The results obtained were normalized to a consistent size to facilitate comparison between experiments and across subjects. This was achieved by defining reference lines on the three-dimensional interpolated data that resulted from the analysis described above. Reference lines were drawn manually along the dorsal, ventral, left and right edges of the cord, overlying axial, sagittal, and coronal slices of the volume data. Approximate boundaries of the spinal cord segments were identified by means of the positions of dorsal nerve roots, and the shapes and sizes of the spinous pro-

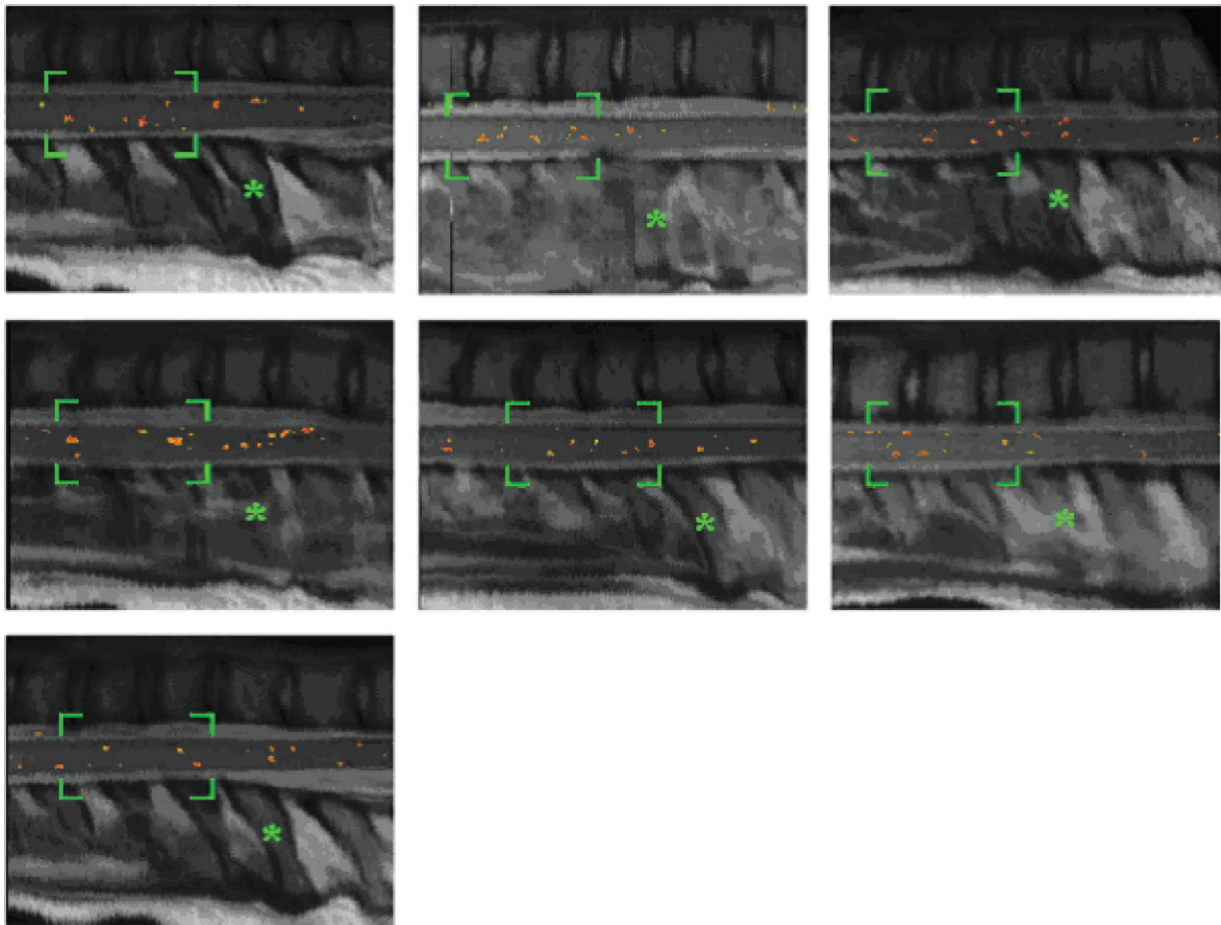


**Figure 1.** Examples of results from seven subjects, showing a single 0.5-mm-thick (interpolated) sagittal slice through the dorsal and ventral gray matter on the right side of the body. Images are oriented with the rostral direction to the left, and the dorsal side is toward the bottom of the frames. Voxels with signal intensity time courses that are significantly correlated with the time course of thermal stimulation are shown in color, overlying the grayscale background. Sensory activity is therefore seen in the lower half of the spinal cord, whereas motor activity is seen in the upper regions. The same rectangular region of the spinal cord in each subject, containing the dominant activity, is indicated by the green corner marks. The spinous process of the seventh cervical vertebra is marked with a green asterisk in each image, and corresponds approximately to the level of the eighth cervical spinal cord segment. The results shown in these images have not been normalized to consistent dimensions.

cesses, as references. Using these manually-defined references, the spinal cord image data and the correlation T-value map were normalized by linear interpolation and translation to a cord cross-section of  $18 \times 30$  pixels (A/P  $\times$  L/R) at each S/I location. Each spinal cord segment was then normalized to be 30 pixels long. Activation maps were produced by thresholding the T-value maps at  $T \geq 2$  to identify active voxels, which were labeled in color, overlying the averaged and normalized reference image data. Image data spanning 210 pixels in the S/I direction therefore spans spinal cord segments C4 to T2 with a width of 30 pixels each.

In order to allow a comparison to be made with the previously employed axial-slice method, the data that had been resliced into 0.5-mm-thick transverse slices was averaged across blocks of 15 slices to create a data set of 7.5-mm-thick transverse slices. The correlation with the model paradigm was again calculated with this data and active voxels were identified, with a T-value threshold of 2.0. The signal intensity time courses of the active voxels in the spinal cord that would have

been determined with the axial-slice method were thus determined.

## RESULTS

Spinal fMRI data obtained from seven volunteers with thermal stimulation of the right hand demonstrated consistent patterns of activity (Fig. 1). The three-dimensional distribution of activity is demonstrated in normalized results in Fig. 2. In the dorsal gray matter ipsilateral to the stimulus, active regions were observed at typically three to five locations at the levels of the fifth, sixth, and seventh cervical vertebrae, corresponding approximately with the sixth, seventh, and eighth cervical spinal cord segments, respectively. In each experiment, the activity was observed at numerous locations within each spinal cord segment with small ( $\sim 2$ -mm) spatial extent in the S/I direction. In ventral gray matter, active areas were also observed and were slightly offset from those in dorsal regions, and in dorsal and ventral gray matter the pattern appeared to

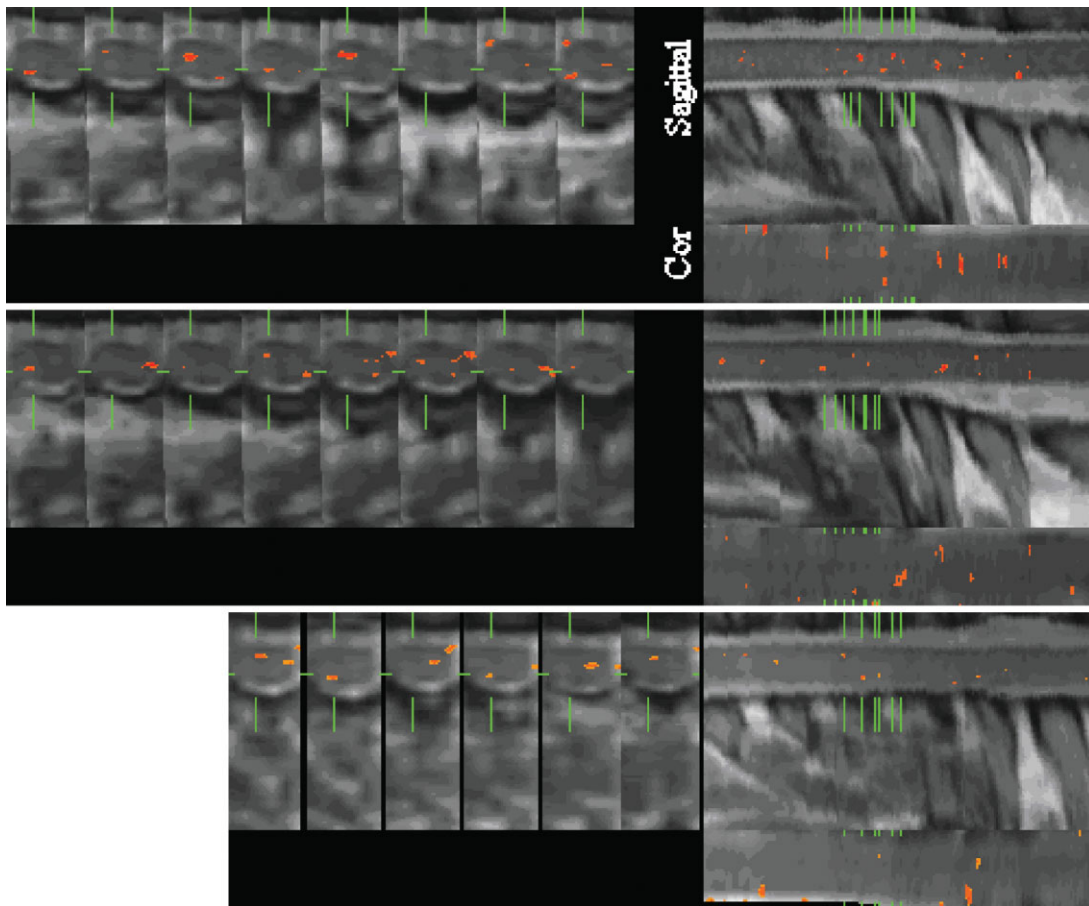


**Figure 2.** Examples of normalized results selected from three subjects, showing a number of axial slices (left side), and one sagittal and coronal slice for each subject (as indicated in the top frame). The positions of the axial slices are indicated in the sagittal and coronal views with green lines, and the positions of the sagittal and coronal slices are indicated in each axial slice. Axial slices are in radiological orientation with the right side of the bottom toward the left side of the frame, and dorsal is toward the bottom. Sagittal and coronal slices are oriented with rostral toward the left. Dorsal is toward the bottom in the sagittal slice, and the right side of the body is toward the top of the coronal slices. The axial slices are in order from rostral to caudal, from left to right, and demonstrate the alternated pattern of dorsal (sensory) and ventral (motor) activity within a single spinal cord segment.

alternate along the rostral–caudal direction within a segment. Activity was observed in both ipsilateral and contralateral ventral gray matter, each slightly offset in the S/I direction from the other, as well as being consistently offset (~1–2 mm) from that in dorsal regions. Activity was more consistently observed in contralateral ventral regions, however, as compared to that in the ipsilateral ventral regions. Some contralateral activity in dorsal gray matter was also observed at locations that were offset in the S/I direction from that in the ipsilateral dorsal areas. The spatial relationship between the ipsilateral and contralateral ventral activity and the ipsilateral dorsal activity appeared to produce a repeated pattern at more than one location within each active spinal cord segment. There were also noticeable gaps of a few millimeters in width at the approximate segment boundaries, where activity was not observed. Some active regions were also observed in ventral gray matter at higher (fourth to fifth cervical) and lower (first to second thoracic) spinal cord segments. Representative examples of results of one experiment from each of the seven volunteers are shown in Fig. 1. Each figure

shows the activity within an interpolated 0.5-mm-thick sagittal slice through the right side of the spinal cord, and demonstrates both the right dorsal and right ventral activity. The images are oriented with dorsal toward the bottom, and the rostral direction is toward the left side of the frame, as demonstrated by the appearance of the spinous processes. The magnitude of the signal intensity changes in all active regions were observed to be consistent and averaged  $10.0\% \pm 1.0\%$  (mean  $\pm$  SD) as shown in Fig. 3. In comparison, the signal intensity time courses obtained with data reformatted into 7.5-mm-thick transverse slices demonstrated an average signal intensity change of  $6.3\% \pm 0.5\%$  (mean  $\pm$  SD).

## DISCUSSION

The results obtained demonstrate that the spinal fMRI method we have developed can provide full three-dimensional coverage of a 12-cm extent of the cervical spinal cord, with high sensitivity to neuronal-activity-related signal changes. Normalized results shown in Fig. 2 provide examples of the three-dimensional cov-

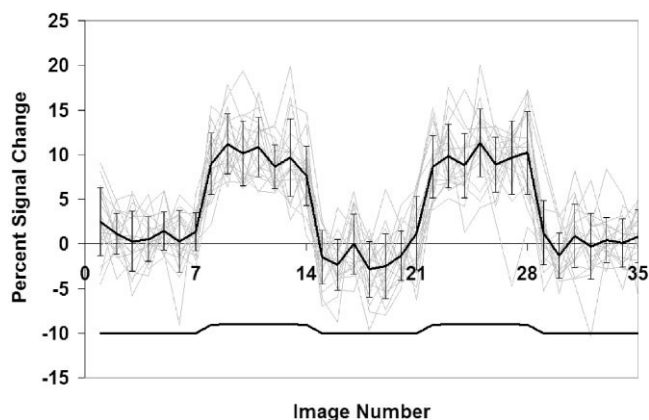


**Figure 3.** Signal intensity time courses of active regions observed in each experiment, plotted in gray. The average time course and errors bars showing the standard deviation are plotted in black. The stimulation paradigm is shown in black at the bottom of the plot.

erage of the cervical spinal cord as any desired transverse, sagittal, and coronal slices can be selected for displaying functional maps. The detail obtained in the data is also demonstrated by the surrounding anatomical features such as spinous processes, which can be clearly identified and used as landmarks for the position in the cord.

The pattern of activity observed in the present study was identical to that observed previously in its R/L and A/P distribution, but differences were notable in the S/I distribution as a result of the finer resolution obtained. The sensory dermatomes on the palm of the hand are known to be innervated from the sixth to the eighth cervical spinal cord segments, corresponding with the observed location of activity. There are also projections to motor areas in the same segment and adjacent segments, and if a stimulus is of sufficient type and intensity, a motor reflex to withdraw from the stimulus can be triggered. However, descending input from the brain can inhibit the reflex. In the present study, the volunteers did not move their arms or hands when the 15°C cold stimulus was applied. Nonetheless, in this study and previous studies with the same stimulus, motor activity was observed in ventral gray matter regions and around the central canal. Both the dorsal and ventral activity was also observed in every experiment to occur at multiple localized regions within a segment, demonstrating a finer-scale organization at the subsegmental level. Similar fine-scale structure has been demonstrated in electrophysiological studies in rats (22). However, this is the first time this structure detail has been observed with spinal fMRI. The areas of ventral activity on the right and left sides were observed to be consistently offset in the S/I direction from the dorsal activity as well as being slightly offset from each other, and the locations of activity in these three areas (right ventral, left ventral, right dorsal) were repeatedly observed in the same pattern. Examples of this pattern are shown in Fig. 2.

Partial volume effects do not appear to be significant with the 2.8-mm-thick sagittal slices employed for this

study because very little contamination from CSF flow is apparent in the results. Such a contribution would be expected to appear as false positive activations around the edges of the cord and should be easily recognized. The effective size of the resolution element ("resel") (23) we have obtained with the sagittal-slice method is approximately  $2.8 \times 0.9 \times 1.8$  mm (R/L  $\times$  A/P  $\times$  S/I) because the smoothing was applied only in the S/I direction across three voxels that were first interpolated to 0.5 mm across, from an original resolution of 0.9 mm. We therefore approximate that we are mixing signal across two original voxels (i.e., 1.8 mm). These resel dimensions are expected to be a closer match to the dimensions of gray matter functional volumes than with the axial-slice method (resel size of approximately  $0.9 \times 0.9 \times 7.5$  mm). At the same time, the effective resel volume and signal-to-noise ratio are maintained at similar values. The interpolation and reslicing applied prior to analysis does not alter the resolution obtained in the original image data. The resolution obtained in the A/P and R/L directions was clearly adequate to demonstrate regions of dorsal and ventral gray matter in the image data. Moreover, partial volume effects in the S/I direction were notably reduced compared to the method described previously with axial slices (5,6), as evidenced by the fact that the fractional signal intensity changes were significantly greater in the present study. Signal changes averaged  $10.0\% \pm 1.0\%$  during stimulation periods with sagittal slices, as compared to  $6.4\% \pm 1.3\%$  under the same stimulation conditions in previous studies, but with axial slices. Reformatting the data obtained in the present study into 7.5-mm axial slices to simulate the data obtained with the axial-slice method, yielded signal intensity changes of  $6.3\% \pm 0.5\%$ . This is consistent with the observation that the active regions each span only a few millimeters in the S/I direction, and so the magnitude of signal change would have been reduced when averaged over the 7.5-mm-thick axial slices used previously. This signal change magnitude is much too large to be attributed to the BOLD effect, and is consistent with the proposed SEEP contrast mechanism being dominant in spinal fMRI (4).

The observation of small, localized areas of activity within the gray matter in each spinal cord segment that is related to sensory dermatomes being stimulated, the correspondence of the observed areas of activity with known neuroanatomy, and the relatively high signal intensity changes, all demonstrate a high degree of sensitivity with the sagittal-slice method described in the present study. This method is therefore expected to provide better sensitivity to neuronal-activity-induced signal changes than was obtained with the previous axial-slice method. The sensitivity and reliability of the sagittal slice method are demonstrated by the consistency of the results obtained, both in repeated experiments with each subject, and across different subjects, and is demonstrated in Figs. 1 and 4. Figure 4 shows maps indicating the reproducibility of the results, which were created at each voxel in the spinal cord by computing the inverse of the average distance to the nearest active voxel, after normalizing the results to consistent dimensions. For example, if at a given voxel

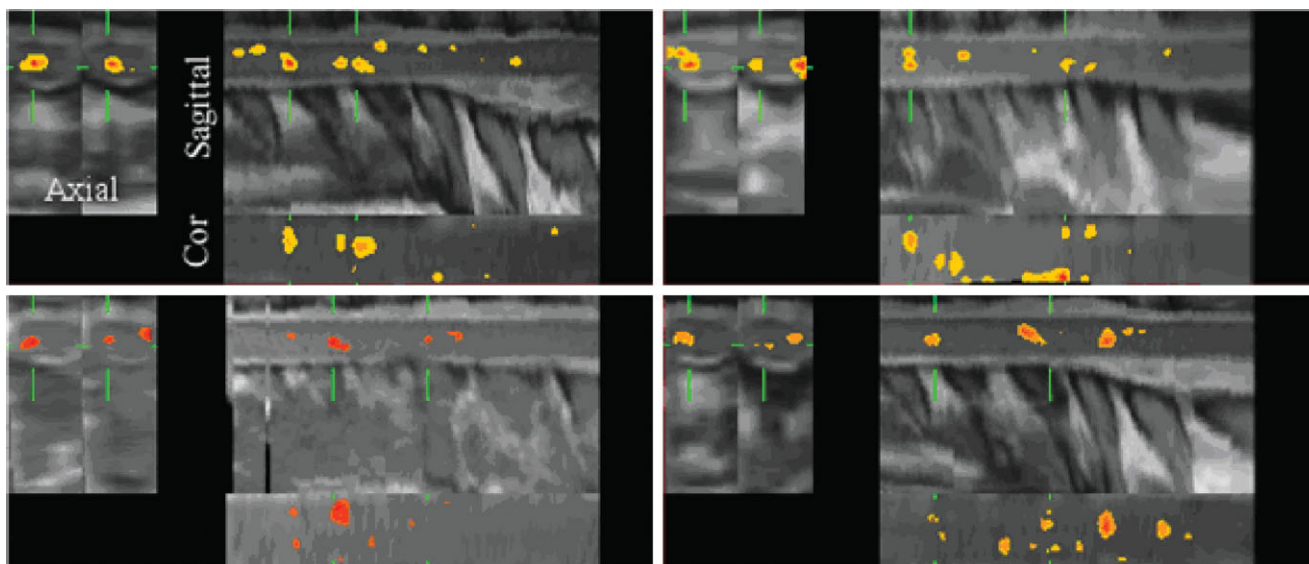


**Figure 4.** Maps indicating reproducibility in repeated experiments with each of four selected subjects, with data normalized to a consistent size and position as described in the text. Colors indicate the inverse of the average distance to the nearest active voxel in each experiment, spanning from red (lowest distance) through orange to yellow (indicating an average distance of three pixels). Average distances above three pixels (inverse value of  $1/3$ ) are not displayed. Each figure shows one 0.5-mm-thick sagittal slice through the right side of the spinal cord, one coronal slice through the dorsal region of the cord, and two selected axial slices. Axial slices are in radiological orientation with the left side of the body on the right side of the image frame. Sagittal slices are shown with the rostral direction to the left, and dorsal is down. Coronal slices are shown with the rostral direction to the left, and the right side of the body is toward the top of the frame. The green lines indicate the positions of the intersecting slices that are shown. Reproducibility was compared across: (top left) two experiments, (top right) two experiments, (bottom left) five experiments, and (bottom right) four experiments.

the average distance to the nearest active voxel in each repeated study was three voxel-widths (the voxel width is 0.5 mm in the normalized data), then that voxel in the reproducibility map would be assigned a value of  $1/3$ . If the average distance was zero, meaning that every set of results being compared showed activity at that location, then the voxel in the reproducibility map was arbitrarily assigned a value of 10. Higher values thus indicate the locations of highly clustered active voxels in repeated experiments. In comparison, Fig. 1 contains images demonstrating the distribution of activity in single experiments for each of the seven volunteers studied, through one selected 0.5-mm-thick sagittal slice through the right side of the spinal cord. The same segmental level of the spinal cord is indicated in each image with green corner marks. Figures 1 and 4 demonstrate highly reproducible areas of activity across repeated studies in each subject, and also show reproducibility in the pattern and locations of activity across different subjects. However, it is important to note that some differences between subjects are to be expected because the distribution of sensory dermatomes varies between individuals, and the thermode used for stimulation did not rest within the palm of each volunteer's hand in precisely the same way. In repeated experiments for each subject it is expected that the thermode position was consistent.

The benefits of carrying out spinal fMRI with thin sagittal slices, and postprocessing to improve the signal-to-noise ratio (by means of averaging across consistent tissue types) are the increased spatial coverage of the spinal cord, greater flexibility in how results can be

displayed, and the improved spatial resolution in the S/I direction. An added benefit of acquiring data in sagittal slices to span a continuous three-dimensional volume is that it is possible to normalize the data to constant dimensions to facilitate viewing of the results, and comparison of results within, or across, subjects. The results shown in Figs. 2 and 4 have been normalized using the method described above and demonstrate the effectiveness of the method. This is the first attempt at defining a normalization technique for spinal cord image data, and more detailed studies are required to determine the optimum normalization for all situations.

In conclusion, a new method for spinal fMRI acquisition with thin sagittal slices, and postprocessing to attain an adequate signal-to-noise ratio, has been demonstrated. Compared to data obtained with axial slices, this method has been shown to provide at least equal sensitivity and reliability, with significantly greater resolution in the S/I direction, to demonstrate a larger extent of the spinal cord, and to yield effectively three-dimensional data. We have also demonstrated the ability to normalize the spinal fMRI data, and produce consistent R/L and A/P dimensions along the cord length. Moreover, with the larger volume imaged with sagittal slices it is possible to identify approximate boundaries of spinal cord segments based on the shape/size of the spinous processes and positions of nerve roots. The sagittal-slice method we have developed for spinal fMRI, therefore, provides a tool that is practical, and better suited for routine use for clinical assessment and spinal cord research.

## ACKNOWLEDGEMENTS

We gratefully acknowledge helpful input from Dr. Spyros Kollias, Dr. Boguslaw Tomanek, and Dr. Krisztina Maliszka. This work was undertaken, in part, thanks to funding from the Canada Research Chairs Program (to P.W.S.).

## REFERENCES

1. Yoshizawa T, Nose T, Moore GJ, Sillerud LO. Functional magnetic resonance imaging of motor activation in the human cervical spinal cord. *Neuroimage* 1996;4:174–182.
2. Stroman PW, Ryner LN. Functional MRI of motor and sensory activation in the human spinal cord. *Magn Reson Imaging* 2001;19:27–32.
3. Stroman PW, Krause V, Maliszka KL, Frankenstein UN, Tomanek B. Functional magnetic resonance imaging of the human cervical spinal cord with stimulation of different sensory dermatomes. *Magn Reson Imaging* 2002;20:1–6.
4. Stroman PW, Krause V, Maliszka KL, Frankenstein UN, Tomanek B. Extravascular proton-density changes as a non-BOLD component of contrast in fMRI of the human spinal cord. *Magn Reson Med* 2002;48:122–127.
5. Stroman PW, Tomanek B, Krause V, Frankenstein UN, Maliszka KL. Mapping of neuronal function in the healthy and injured human spinal cord with spinal fMRI. *Neuroimage* 2002;17:1854–1860.
6. Stroman PW, Kornelsen J, Bergman A, et al. Non-invasive assessment of the injured human spinal cord by means of functional magnetic resonance imaging. *Spinal Cord* 2004;42:59–66.
7. Kollias SS, Kwiecinski S, Summers P. Functional MR Imaging of the human cervical spinal cord. In: *Proceedings of the 42nd Annual Meeting of the American Society of Neuroradiology*, Seattle, June 7–11, 2004. (abstract 227).
8. Brooks J, Robson M, Schweinhardt P, Wise R, Tracey I. Functional magnetic resonance imaging (fMRI) of the spinal cord: a methodological study. In: *Proceedings of the 23rd Annual Meeting of the American Pain Society*, Vancouver, May 6–9, 2004 (abstract 667).
9. Stroman PW, Krause V, Maliszka KL, Frankenstein UN, Tomanek B. Characterization of contrast changes in functional MRI of the human spinal cord at 1.5 T. *Magn Reson Imaging* 2001;19:833–838.
10. Stroman PW, Tomanek B, Krause V, Frankenstein UN, Maliszka KL. Functional magnetic resonance imaging of the brain based on signal enhancement by extravascular protons (SEEP fMRI). *Magn Reson Med* 2003;49:433–439.
11. Stroman PW, Maliszka KL, Onu M. Functional magnetic resonance imaging at 0.2 tesla. *Neuroimage* 2003;20:1210–1214.
12. Piet R, Vargova L, Sykova E, Poulain DA, Oliet SH. Physiological contribution of the astrocytic environment of neurons to intersynaptic crosstalk. *Proc Natl Acad Sci USA* 2004;101:2151–2155.
13. Svoboda J, Sykova E. Extracellular space volume changes in the rat spinal cord produced by nerve stimulation and peripheral injury. *Brain Res* 1991;560:216–224.
14. Sykova E, Vargova L, Kubinova S, Jendelova P, Chvatal A. The relationship between changes in intrinsic optical signals and cell swelling in rat spinal cord slices. *Neuroimage* 2003;18:214–230.
15. Sykova E, Vargova L, Prokopova S, Simonova Z. Glial swelling and astrogliosis produce diffusion barriers in the rat spinal cord. *Glia* 1999;25:56–70.
16. Sykova E. Modulation of spinal cord transmission by changes in extracellular K<sup>+</sup> activity and extracellular volume. *Can J Physiol Pharmacol* 1987;65:1058–1066.
17. Stroman PW, Nance PW, Ryner LN. BOLD MRI of the human cervical spinal cord at 3 tesla. *Magn Reson Med* 1999;42:571–576.
18. Porszasz R, Beckmann N, Bruttel K, Urban L, Rudin M. Signal changes in the spinal cord of the rat after injection of formalin into the hindpaw: characterization using functional magnetic resonance imaging. *Proc Natl Acad Sci USA* 1997;94:5034–5039.
19. Madi S, Flanders AE, Vinitski S, Herbison GJ, Nissanov J. Functional MR imaging of the human cervical spinal cord. *AJNR Am J Neuroradiol* 2001;22:1768–1774.
20. Backes WH, Mess WH, Wilmlink JT. Functional MR imaging of the cervical spinal cord by use of median nerve stimulation and fist clenching. *AJNR Am J Neuroradiol* 2001;22:1854–1859.
21. Lawrence J, Stroman PW, Bascaramurty S, Jordan LM., Maliszka KL. Correlation of functional activation in the rat spinal cord with neuronal activation detected by immunohistochemistry. *Neuroimage* 2004;22:1802–1807.
22. Takahashi Y, Chiba T, Kurokawa M, Aoki Y. Dermatomes and the central organization of dermatomes and body surface regions in the spinal cord dorsal horn in rats. *J Comp Neurol* 2003;462:29–41.
23. Worsley KJ, Friston KJ. Analysis of fMRI time-series revisited—again. *Neuroimage* 1995;2:173–181.